

Bent-shaped mesogens without an azomethine joint

Jozef Mieczkowski,^a Jadwiga Szydłowska,^{*a} Joanna Matraszek,^a Damian Pocięcha,^a
Ewa Gorecka,^{a,b} Bertrand Donnio^b and Daniel Guillon^b

^aDepartment of Chemistry, Warsaw University, Al. Zwirki i Wigury 101, 02-089 Warsaw, Poland. E-mail: jadszyd@chem.uw.edu.pl; Fax: +48 22 8221075; Tel: +48 22 8221075

^bInstitut de Physique et Chimie des Matériaux de Strasbourg, Groupe des Matériaux Organiques, 23 rue du Loess, 67037 Strasbourg Cedex, France

Received 24th May 2002, Accepted 19th August 2002

First published as an Advance Article on the web 12th September 2002

A new series of banana-shaped mesogens with ethylene links in the branches and laterally substituted are presented. They form B₁, B₂, B₆ and B₇-like phases. The B₇-like and B₂ phases are not miscible although identical crystallographic structures are deduced from X-ray studies. The switching in the B₇-like phase is without a threshold and occurs only in a small number of domains. Dielectric measurements do not confirm ferroelectric properties for the B₇-like phase, and only a weak non-collective relaxation process was observed. In the B₂ phase a collective and weak dielectric mode was detected. The B₁ phase exhibits a columnar structure with a large rectangular cell 111.6 × 51 Å².

Introduction

In recent years a large number of substances made of V-shaped (banana) molecules and revealing liquid crystalline properties have been synthesised and studied. They form a new class of thermotropic mesogens that exhibit polar mesophases.^{1–4} Most of the reported compounds are resorcinol derivatives, symmetrically substituted at the 1 and 3 positions. Biphenyl,⁵ terphenyl,³ naphthalene⁶ and other symmetric and non-symmetric bent structures have also been presented.⁷ The central ring has been additionally substituted at the available positions by a chlorine or bromine atom, a nitro, methyl or even hexyl group.^{8–11} The branches of the banana molecule have usually contained two or three phenyl rings joined directly¹² or connected through ester, imino or vinylic groups. The phenyl rings of the branches have been substituted at different positions by fluorine^{6,13,14} and chlorine^{15,16} atoms and methyl groups. Then alkoxy or alkyl chains have been attached at the terminal positions of the molecules.

Most of the synthesised banana-shaped compounds contain in their structures the imino (-N=CH-) linking group, which is sensitive to air and moisture and causes decomposition in a short time. In this work, we present five new homologous series of banana-shaped compounds that do not contain this azomethine group. They are symmetric five rings resorcinol derivatives, with the branches being attached to the central phenyl ring *via* carboxy (-C(O)-O-) groups (Scheme 1, series 1–5). The branches contain two phenyl rings connected by ethenyl linking groups and terminated at the *para* position by alkoxy chains of different lengths. The external *p*-alkoxyphenyl moiety of the branches was broadened by a lateral *meta* chloro-, bromo-, nitro, methoxy- or other substituent. The main resorcinol ring was also modified by the attachment of a methyl group at the 2- (series 2) or 5-position (series 3). Compounds of the series 1 have no additional substituents at the central ring. The compounds of series 1–3 reveal mainly B₇ or B₂ liquid crystalline phases. In the compounds of series 4, the substituent attached at the 5-position of the central ring is a pentyl chain. The central rings of the molecules of series 5 are asymmetrically substituted at the 4-position by alkyl or ester chains.

In this paper, we report on the structural characterization and dielectric measurements of the mesomorphic phases exhibited by these new series of banana-shaped molecules.

Experimental

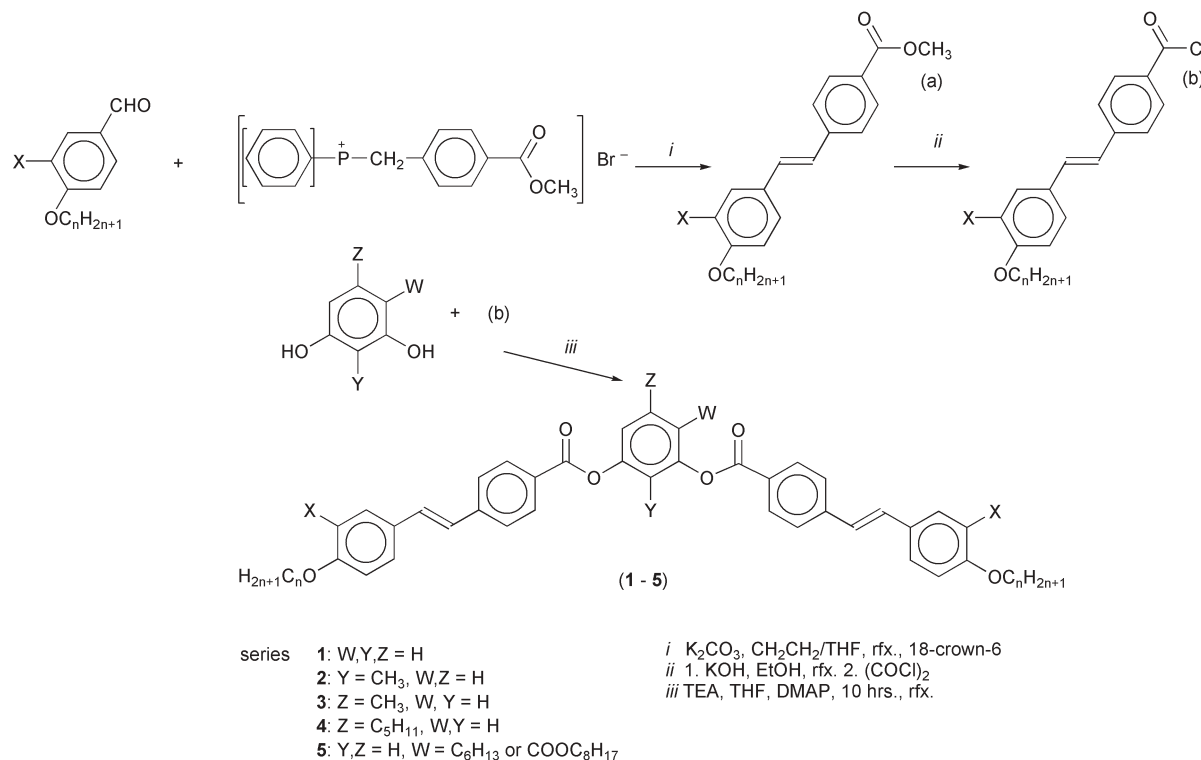
Mesophase identification was based on microscopic routine examination of the textures formed by samples between two glass plates or in free suspended films. A Zeiss Jenapol-U polarising microscope equipped with a Mettler FP82HT hot stage was used. The structure of the detected LC phases was supported by X-ray studies carried out on powder samples in Lindemann capillaries. The patterns were registered with an Inel CPS 120 curved positional sensitive counter and confirmed with a Gunier set-up. The sample temperature was controlled to within 0.1 K.

The phase transition temperatures were mainly determined by calorimetric measurements performed with a Perkin-Elmer DSC-7 apparatus. When a LC phase was monotropic or a transition temperature was too high, the phase transition point was taken from microscopic observations.

The birefringence was estimated in cells of 2–6 μm by comparison with tabulated interference colours of a quartz wedge between crossed polarisers in white light. The intensity of light transmitted through the sample was taken by a microphotometry system Nikon P102 attached to the polarising microscope Optiphot2-Pol. The changes in sample textures under electric field, spontaneous polarisation and dielectric dispersion measurements were studied in glass cells 2 and 4 μm thick. They were prepared from glass plates coated with ITO transparent electrodes and carrying a rubbed planar surfactant, separated by Mylar spacers. The dielectric dispersion studies were performed with a Wayne Kerr Precision Component Analyser 6425 in the frequency range 20 Hz–300 kHz. The relaxation frequency f_r and the strength $\Delta\epsilon$ of the dielectric modes were obtained by fitting the complex permittivity $\epsilon^*(\omega) = \epsilon' - i\epsilon''$ to the Cole–Cole dispersion law:

$$\epsilon^* - \epsilon_\infty = \frac{\Delta\epsilon}{1 + (if/f_r)^{(1-\alpha)}} - i \frac{\sigma}{2\pi\epsilon^0 f}$$

where α , ϵ_∞ , σ and ϵ^0 are the distribution parameter of the mode, the high frequency permittivity, the conductivity of the sample and the permittivity of the vacuum, respectively. Spontaneous polarisation was measured using the switching current method under triangular wave voltage. Molecular dimensions were estimated by molecular modelling (HYPERCHEM).



Scheme 1

To confirm the molecular structure of the synthesised compounds the following analytical methods were applied. Infrared (IR) spectra were obtained using a Nicolet Magna IR 500 spectrophotometer. ^{13}C NMR spectra were recorded on a Varian Unity Plus spectrometer operating at 125 MHz, whereas ^1H NMR spectra were recorded at 200 MHz or at 500 MHz when high signal separation was necessary. Tetramethylsilane was used as an internal standard. Chemical shifts are reported in ppm. TLC analyses were performed on Merck 60 silica gel glass plates and visualised using iodine vapour. Column chromatography was carried out at atmospheric pressure using silica gel (100–200 mesh, Merck). Compositions of the synthesised compounds, determined by elemental analysis, confirmed the expected molecular structures.

Synthesis

The synthetic route to the described compounds is sketched in Scheme 1.

3-Chloro-4-(dodecyloxy)benzaldehyde ($n = 12$). Anhydrous potassium carbonate (30 g, 0.22 mol) and dodecyl bromide (60 g, 0.24 mol) were added to 3-chloro-4-hydroxybenzaldehyde (32 g, 0.2 mol) dissolved in dimethylformamide (200 ml). The reaction mixture was heated at 120 °C for 12 hours, then poured into water and the crude product was extracted with toluene. The toluene layer was dried with anhydrous magnesium sulfate and after evaporation of the solvent the product was distilled under reduced pressure (bp 270 °C/10 Torr) and slowly solidified in a refrigerator (mp 55–57 °C; 45.5 g, 68.5%).

Elemental analysis for $\text{C}_{12}\text{H}_{29}\text{O}_2\text{Cl}$ ($M = 324.5$): calc. C 70.26, H 8.93; found C 70.01, H 9.01%; IR ν_{max} (KBr)/ cm^{-1} : 2950, 2940, 2918, 2845, 1695, 1600, 1580, 1500, 1490, 1290, 1200, 1050, 820; ^1H NMR $\delta_{\text{H}}(\text{CDCl}_3)$: 8.941 (s, 1H), 7.899 (d, 1H, $J = 2.0$ Hz), 7.44 (dd, 1H, $J_1 = 2.0$ Hz, $J_2 = 8.3$ Hz), 7.013 (d, 1H, $J = 8.4$ Hz), 4.115 (t, 3H), 1.879 (m, 2H), 1.492 (m, 2H), 1.266 (m, 18H), 0.880 (t, 3H); ^{13}C NMR $\delta_{\text{C}}(\text{CDCl}_3)$: 189.869, 159.670, 131.394, 130.578, 130.133, 124.088, 112.594, 69.684, 32.069, 29.789, 29.716, 29.665, 29.498, 29.418, 29.010, 26.023, 22.840, 14.274.

4-[(*E*)-2-[3-Chloro-4-(dodecyloxy)phenyl]ethenyl]benzoic acid methyl ester (a) ($n = 12$). Anhydrous potassium carbonate (13.8 g, 0.1 mol) and 18-crown-6 (100 mg) were added to phosphonium salt (methyl 4-(triphenylphosphoniomethyl)benzoate bromide) (34 g, 0.0692 mol) dissolved in dry methylene dichloride (300 ml) and mixed at room temperature for about one hour. 3-Chloro-4-(dodecyloxy)benzaldehyde (21 g, 0.0647 mol) dissolved in tetrahydrofuran (200 ml) was added to the yellow reaction mixture which was heated under reflux for 30 hours. After the inorganic salts were filtered, the filtrate was evaporated to dryness and methanol was added to the remaining oil, from which the product (a) crystallized slowly (mp 69–71 °C; 12.4 g, 42.2%). According to the spectral data, only (*E*)-stilbene was crystallized from the reaction mixture.

Elemental analysis for $\text{C}_{28}\text{H}_{37}\text{O}_3\text{Cl}$ ($M = 456.5$): calc. C 73.60, H 8.10; found C 73.49, H 8.25%; IR ν_{max} (KBr)/ cm^{-1} : 2940, 2910, 2850, 1720, 1510, 1500, 1455, 1420, 1290, 1100, 980; ^1H NMR $\delta_{\text{H}}(\text{CDCl}_3)$: 8.004 (d, 2H, $J = 8.3$ Hz), 7.556 (d, 1H, $J = 1.8$ Hz), 7.514 (d, 2H, $J = 8.5$ Hz), 7.319 (dd, 1H, $J_1 = 2.0$ Hz, $J_2 = 8.4$ Hz), 7.017 (d, 2H, $J = 9.8$ Hz), 6.886 (d, 1H, $J = 8.8$ Hz), 4.029 (t, 3H), 3.991 (s, 3H), 1.839 (m, 2H), 1.476 (m, 2H), 1.264 (m, 18H), 0.880 (t, 3H); ^{13}C NMR $\delta_{\text{C}}(\text{CDCl}_3)$: 167.020, 154.753, 141.897, 130.359, 130.199, 129.711, 128.939, 128.283, 126.666, 126.593, 126.302, 123.527, 113.358, 69.421, 52.224, 32.091, 29.818, 29.760, 29.724, 29.512, 29.228, 26.103, 22.862, 14.296.

4-[(*E*)-2-[3-Chloro-4-(dodecyloxy)phenyl]ethenyl]benzoic acid chloride (b) $n = 12$. Potassium hydroxide (2 g, 0.0357 mol) was added to methyl ester (a) (12 g, 0.0262 mol) dissolved in hot ethanol, and the reaction mixture was heated under reflux for 24 hours. After cooling, the potassium salt (10 g) was crystallized, then dried under vacuum over phosphorus pentoxide suspended in toluene, then treated with excess of oxalyl chloride (10 ml). The reaction mixture was heated for 8 hours under reflux. After filtration of precipitated potassium chloride, the solvent was evaporated to dryness. The product (b) slowly solidified at room temperature (8 g).

3-[4-((E)-2-[3-Chloro-4-(dodecyloxy)phenyl]ethenyl]benzoyloxy]-phenyl 4-((E)-2-[3-chloro-4-(dodecyloxy)phenyl]ethenyl]benzoate (1), X = Cl, n = 12. Triethylamine (10 ml), DMAP (50 mg) and the chloride (b) (4.5 g, 0.00976 mol) were added to resorcinol (0.5 g, 0.00454 mol) dissolved in dry methylene dichloride (50 ml). The reaction mixture was heated under reflux for 8 hours, then the excess of the solvents was evaporated and the remaining oil was chromatographed on silica gel eluted with methylene dichloride. The crude product was recrystallized twice from ethyl acetate (2.1 g, 48.2%).

Elemental analysis for $C_{60}H_{72}O_6Cl_2$ ($M = 959$): calc. C 75.07, H 7.50; found C 75.18, H 7.65%; IR ν_{max} (KBr)/ cm^{-1} : 2950, 2920, 2850, 1720, 1600, 1500, 1490, 1290, 1240, 1110, 1050, 1010; 1H NMR (500 MHz) $\delta_H(CDCl_3)$: 8.148 (d, 4H, $J = 8.5$ Hz), 7.568 (m, 6H), 7.465 (t, 1H), 7.333 (dd, 2H, $J_1 = 2.0$ Hz, $J_2 = 8.0$ Hz), 7.199 (t, 1H), 7.164 (dd, 2H, $J_1 = 2.0$ Hz, $J_2 = 8.0$ Hz), 7.111 (m, 2H), 6.988 (m, 2H), 6.895 (d, 2H, $J = 8.0$ Hz), 4.029 (t, 4H), 1.837 (m, 4H), 1.486 (m, 4H), 1.40–1.20 (m, 36H), 0.881 (t, 6H); ^{13}C NMR $\delta_C(CDCl_3)$: 164.252, 154.680, 151.479, 142.552, 130.676, 130.064, 130.062, 130.032, 129.806, 128.713, 127.747, 126.551, 126.318, 126.289, 123.353,

119.199, 115.845, 113.146, 69.230, 31.927, 29.675, 29.653, 29.599, 29.562, 29.366, 29.348, 29.053, 25.939, 22.702, 14.143.

Compounds of series **2–5** were prepared similarly except of the use of the central unit (2-methylresorcinol, 5-methylresorcinol, 5-pentylresorcinol (olivetol), 4-hexylresorcinol, 4-octanoyloxyresorcinol).

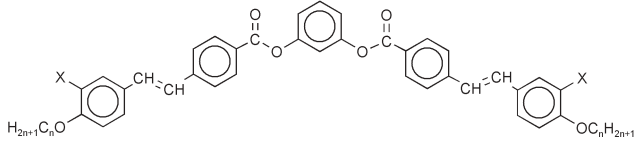
Results and discussion

The phase transition temperatures and the corresponding enthalpies are collected in . The phase diagrams of the series **1–3** are shown in Fig. 1.

Series 1—B₇-like phase

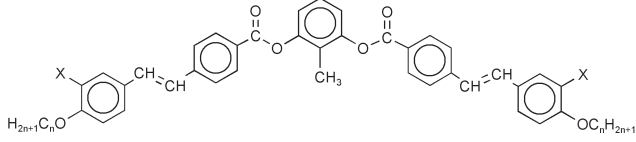
Compounds of series **1** exhibit the enantiotropic liquid crystalline phase whose microscopic textures are similar to those of the B₇ phase described previously.^{8,9,15} Upon cooling from the isotropic phase a characteristic tiny ‘spiralling’ germ texture appears. When the temperature is lowered rather slowly a variety of domains are created that resemble B₇ phase

Table 1 Phase sequence, phase transition temperatures ($^{\circ}C$) and enthalpy changes (in parentheses, $J g^{-1}$) for compounds of series **1**

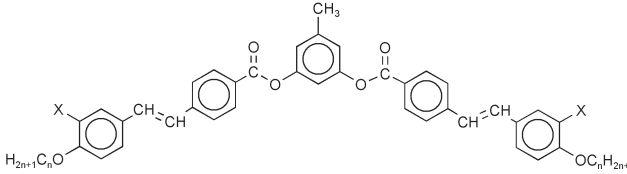
|  | | | | | | |
|--|-----------------------------------|-----|---------------|---|--------------|-----|
| <i>n</i> | X | Cry | | LC phases | | Iso |
| 12 | H | ● | 182.9 (11.3) | Unknown | ~200 dec | ● |
| 8 | Cl | ● | 124.8 (24.6) | B ₇ -like | 139.7 (18.9) | ● |
| 9 | Cl | ● | 121.7 (20.4) | B ₇ -like | 137.4 (15.8) | ● |
| 10 | Cl | ● | 118.0 (20.8) | B ₇ -like | 140.4 (17.9) | ● |
| 11 | Cl | ● | 115.5 (19.1) | B ₇ -like | 136.6 (18.8) | ● |
| 12 | Cl | ● | 116.4 (18.9) | B ₇ -like | 144.4 (18.2) | ● |
| 15 | Cl | ● | 107.1 (16.6) | B ₇ -like | 137.6 (16.2) | ● |
| 12 | Br | ● | 118.3 (18.5) | B ₇ -like | 131.3 (15.6) | ● |
| 12 | NO ₂ | ● | 141.8 (28.0) | B ₁ – 149.8 (1.32) – B ₆ | 150.6 (15.0) | ● |
| 8 | OCH ₃ | ● | 85.4 (55.5) | — | — | ● |
| 12 | OCH ₃ | ● | 126.8 (75.3) | — | — | ● |
| 1 | OC ₁₂ H ₂₅ | ● | 105.6 (115.7) | — | — | ● |
| 12 | Br, OCH ₃ ^a | ● | 92.8 (41.3) | — | — | ● |
| 8 ^b | H | ● | 132.3 (52.1) | — | — | ● |

^aBoth *meta* positions are substituted. ^bThe terminal chain is chiral -OCH₂CH(C₂H₅)C₄H₉.

Table 2 Phase sequence, phase transition temperatures ($^{\circ}C$) and enthalpy changes (in parentheses, $J g^{-1}$) for compounds of series **2**

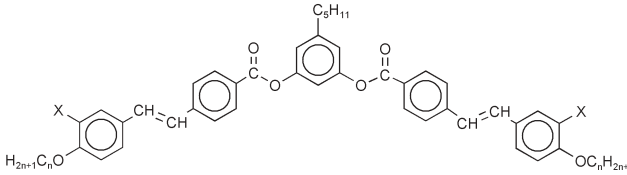
|  | | | | | | |
|--|-----------------------------------|-----|--------------|----------------|--------------|-----|
| <i>n</i> | X | Cry | | B ₂ | | Iso |
| 8 | Cl | ● | 120.4 (48.0) | ● | 117.6 (12.5) | ● |
| 9 | Cl | ● | 108.3 (29.6) | ● | 119.8 (14.1) | ● |
| 10 | Cl | ● | 107.2 (34.5) | ● | 126.0 (12.6) | ● |
| 11 | Cl | ● | 111.6 (41.6) | ● | 121.3 (3.47) | ● |
| 12 | Cl | ● | 129.6 (70.1) | ● | 123.4 (11.2) | ● |
| 15 | Cl | ● | 101.7 (52.8) | ● | 122.7 (12.9) | ● |
| 12 | Br | ● | 127.0 (50.5) | ● | 103.1 (5.6) | ● |
| 12 | NO ₂ | ● | 167.0 (58.2) | — | — | ● |
| 12 | Br, OCH ₃ ^a | ● | 92.1 (19.4) | — | — | ● |
| 12 ^b | Cl | ● | 160.1 (36.4) | — | — | ● |

^aboth *ortho* positions are substituted. ^binstead of CH₃ group in position 2 of central ring NO₂ group is substituted.

Table 3 Phase sequence, phase transition temperatures (°C) and enthalpy changes (in parentheses, J g⁻¹) for compounds of series 3


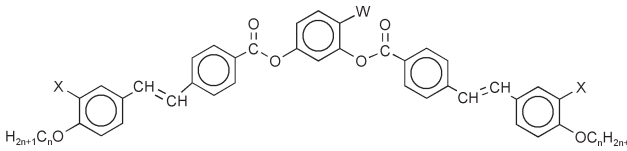
| n | X | Cry | B ₂ | Iso |
|----|-----------------------------------|--------------|----------------|------------------|
| 8 | Cl | 127.7 (83.1) | ● | 103 ^a |
| 9 | Cl | 125.7 (75.7) | ● | 99 ^a |
| 10 | Cl | 126.9 (39.7) | ● | 109 ^a |
| 11 | Cl | 123.5 (36.9) | ● | 104 ^a |
| 12 | Cl | 122.0 (40.6) | ● | 109 ^a |
| 15 | Cl | 117.9 (32.0) | ● | 106 ^a |
| 12 | Br | 134.5 (46.1) | ● | 95 ^a |
| 12 | NO ₂ | 180.6 (51.1) | — | — |
| 12 | Br, OCH ₃ ^b | 80.4 (17.8) | — | — |

^aFrom microscopy. ^bBoth *ortho* positions are substituted.

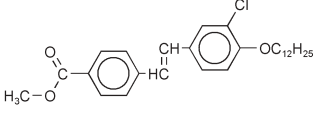
Table 4 Phase sequence, phase transition temperatures (°C) and enthalpy changes (in parentheses, J g⁻¹) for compounds of series 4


| n | X | Cry | Iso |
|----|----|-----|-------------|
| 10 | Cl | ● | 37.4 (27.3) |
| 15 | Cl | ● | 61.3 (30.3) |

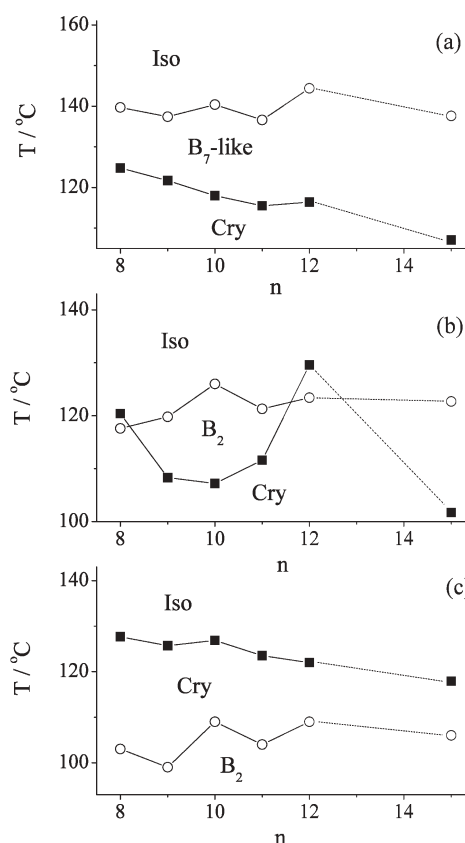
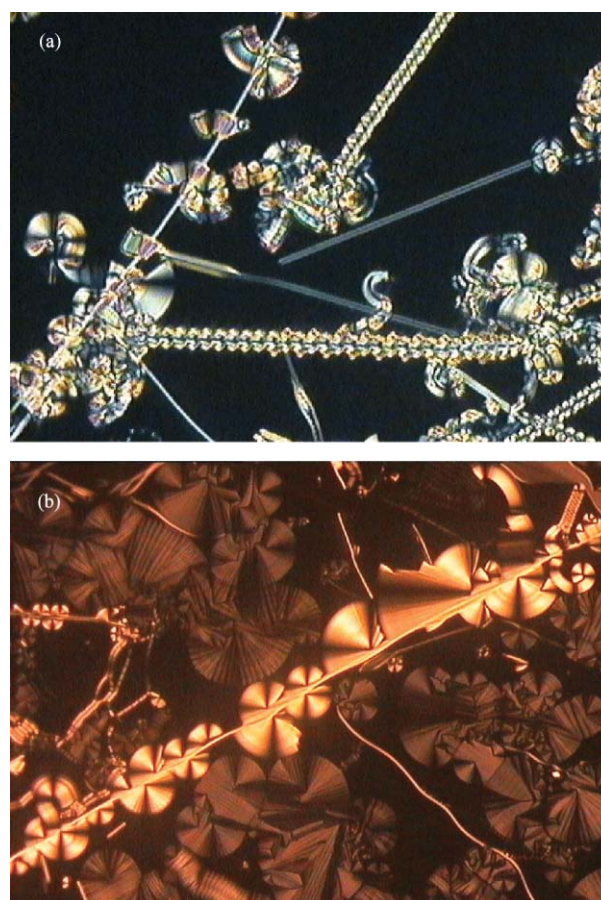
domains (Fig. 2). Among them double-twisted helices, fans or myelinic textures can be observed. However, since there are contradictory reports on the features of the B₇ phase and as there is no clear standard as to what constitutes the B₇ phase,

Table 5 Phase sequence, phase transition temperatures (°C) and enthalpy changes (in parentheses, J g⁻¹) for compounds of series 5


| n | W | X | Cry | N | Iso |
|----|-----------------------------------|----------------------------------|-----|--------------|-----|
| 8 | C ₆ H ₁₃ | OCH ₃ | ● | 111.2 (52.0) | — |
| 12 | C ₆ H ₁₃ | OCH ₃ | ● | 76.6 (56.0) | — |
| 12 | C ₆ H ₁₃ | Br | ● | 47.7 (40.3) | — |
| 1 | C ₆ H ₁₃ | OC ₁₂ H ₂₅ | ● | 46.5 (46.9) | — |
| 12 | COOC ₈ H ₁₇ | Cl | ● | 62.5 (35.3) | ● |
| 12 | COOC ₈ H ₁₇ | Br | ● | 66.4 (35.6) | — |



Cry – 77.2 (50.6) – S_A – 92.7 (4.7) – Iso

**Fig. 1** Phase diagram for the series (a) 1, X = Cl, (b) 2, X = Cl, (c) 3, X = Cl; full squares are melting points and open circles correspond to the isotropization.**Fig. 2** Growth of B₇-like phase domains on cooling the isotropic phase—series 1, X = Cl, (a) n = 11, (b) n = 12.

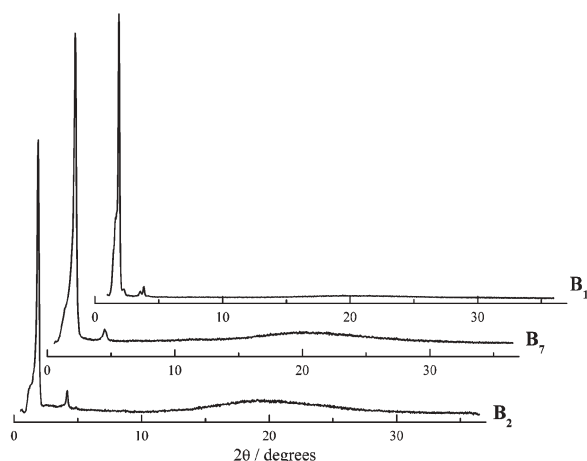


Fig. 3 X-Ray diffraction from a powder sample in the B₂ phase (series 2, $n = 10$, X = Cl), B₇-like phase (series 1, $n = 10$, X = Cl) and B₁ phase (series 1, $n = 12$, X = NO₂). For the B₁ phase, the signal (200) is partially covered by the beam stopper.

we would like to call this phase 'B₇-like'. In a contact preparation between compounds showing the B₇-like phase (series 1, $n = 11$) and the B₂ phase (series 2, $n = 10$), a sharp border between the two phases was observed, indicating a lack of miscibility between them.

In the DSC thermogram, the enthalpy change signal at this point reveals substantial broadening on the side of the B₇-like phase for all compounds. The B₇-like phase exhibits a simple layered structure. The X-ray diffraction pattern (Fig. 3) shows the first and second order signals derived from the layer thickness and a diffuse reflection at 4.5 Å related to the liquid-like order within the layers. In the low angle region no additional incommensurate signals were found. Such additional signals have been reported previously for the B₇ phase and, by some authors, are considered to be the proof of the existence of the B₇ phase.^{8,12,13,17,18} However, it should be noted that the positions of these signals in relation to the signal associated with the layer thickness are not always the same. Additional signals have been found for distances much

shorter,^{12,13,18} or much longer^{13,15} than those giving rise to the main signal. Also splitting of the main layer thickness signal has been reported.^{8,19} For all our compounds the measured layer thickness d is significantly smaller than the longest molecular dimension L , defined by the molecular diagonal, estimated by molecular modelling. This result suggests a molecular plane tilt in the smectic layer. The ratio obtained for all compounds is $d/L \sim 0.8$ which gives a tilt angle $\sim 36^\circ$.

In the microscopic studies (for cells 6 and 2 μm thick), a pale texture containing ribbon structures as well as fan-like circular domains was observed. In addition, some bright circular focal conic domains were created. The birefringence of pale and bright domains was estimated to be $\Delta n < 0.04$ and $\Delta n \sim 0.09$, respectively. These are very low values in comparison to the birefringence of the related compounds of series 3 ($\Delta n = 0.16$) showing the synclitic B₂ phase. The extinction brushes in both types of the circular domains are formed along the directions of the polarisers.

Application of a low frequency a.c. electric field influences the texture. For some small bright circular domains a brush rotation appears⁹ (Fig. 4). A linear reaction to the electric field is observed. The light transmission measured in the bright part of a circular domain, at the edge of the brush, is linearly dependent on the applied triangular wave voltage (Fig. 5). Removing the field pushes the brushes immediately back to their initial orientation. This behaviour could reflect the molecular switching from an anticlinic to a synclitic arrangement. However, the rotation of the brushes is not accompanied by changes of birefringence. Increasing the electric field strength increases the number of circular domains that switch. Once the domains have been switched, they become sensitive even to a low field. The amplitude of motion is different for different domains but is proportional to the applied voltage. The largest recorded tilt was $\sim 28^\circ$. Switching exhibits neither the threshold nor saturation in a broad voltage range, which is similar to the linear electroclinic effect in the smectic A phase of chiral compounds. When the field is sufficiently high ($50 \text{ V}_{\text{pp}} \mu\text{m}^{-1}$), the switchable bright circular domains become, for a short time, yellowish in a sample 2 μm thick or bluish in a sample 4 μm thick, thus they are highly birefringent ($\Delta n = 0.16$) with brushes tilted at about 31° . Then the whole texture, together with the pale parts, is rebuilt into a grainy contrasting texture that is no longer sensitive to the field. No polarisation reversal current peak is observed for any applied voltage, which might suggest that the electric polarisation of the sample is linearly dependent on the electric field or that in the sample there is a relatively small amount of switchable domains.

The dielectric investigation showed only a single, weak, high frequency mode at about 10^5 – 10^6 Hz. The relaxation frequency decreases with decreasing temperature. This mode is observed



Fig. 4 Changes in the extinction brush direction in a small circular domain in the B₇-like phase under an electric field (series 1, $n = 10$, X = Cl; sample 2 μm thick, 0 V and $\sim 10 \text{ V } \mu\text{m}^{-1}$).

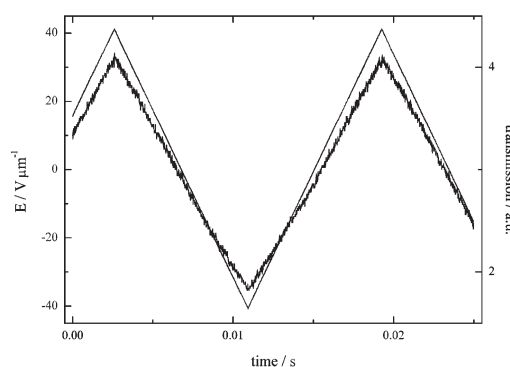


Fig. 5 Light transmission measured for the circular domain in the B₇-like phase at the edge of an extinction brush, serrated curve; solid line, applied electric field (series 1, $n = 10$, X = Cl, temp. 120 °C, sample 2 μm thick).

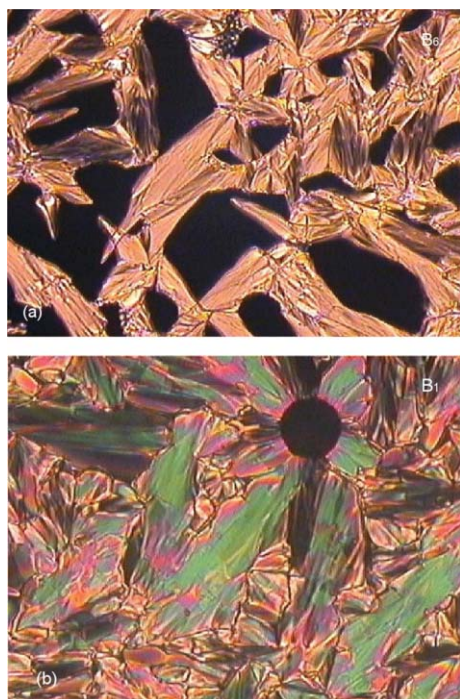


Fig. 6 Texture of (a) the B₆ phase, (b) the B₁ phase (series 1, $n = 12$, X = NO₂).

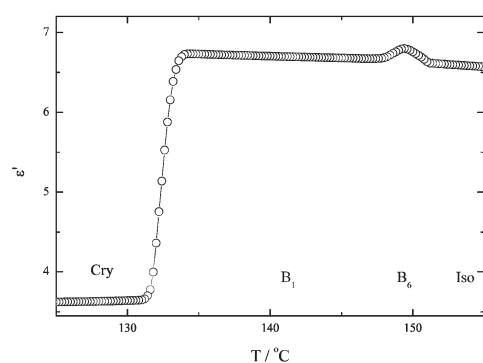


Fig. 7 Temperature dependence of the real part of the dielectric permittivity measured on cooling at 10 kHz for the Iso, B₆ and B₁ phases of compounds of series 1, $n = 12$, X = NO₂.

in the B₇-like phase as well as in the isotropic phase, but disappears in the crystalline phase, and is probably due to a non-collective molecular rotation. The mode strength is $\Delta\epsilon \sim 1-2$ and it slightly increases near the transition temperature between the B₇-like and the isotropic liquid phase.

Concluding, we observe the B₇-like phase whose textures are identical to the B₇ phase textures. However, the B₇-like phase has a layered crystal structure similar to that of the B₂ phase. Simultaneously, the B₇-like phase shows much different electrooptic properties than the antiferroelectric B₂ phase. In the B₇-like phase, switching without a threshold occurs only in some domains.⁹ Moreover, low dielectric permittivity excludes the ferroelectric properties from the B₇-like phase, although they have been reported for the B₇ phase.^{20,21}

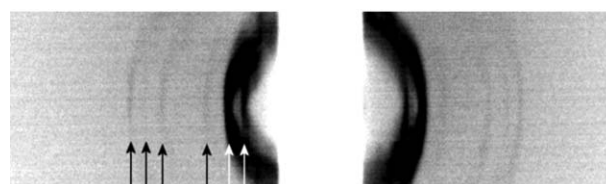


Fig. 8 X-Ray diffraction of a powder sample of the B₁ phase, recorded with a Guinier camera (series 1, $n = 12$, X = NO₂). Arrows indicate signals at 23.02, 24.9, 27.6, 38.1, 46.4 and 55.8 Å.

Series 1—B₁ and B₆ phases

The two phases B₁ and B₆ are exhibited by the compounds of series 1 containing the nitro group at the X position on the outer ring of the branches. The temperature range of the B₆ phase is very narrow, less than 1 °C. The texture formed at the transition from the isotropic liquid forms focal conic defects of low viscosity which is similar to the texture of the smectic A or C phases (Fig. 6a). Attempts to obtain a dark homeotropic texture were unsuccessful which proves that the phase is not the smectic A phase. In the microscopic observations, texture changes are visible at the transition temperature to the B₁ phase only in thick cells, while the fan-shaped texture remains almost unchanged (Fig. 6b) in thin cells. The extinction brushes—the dark area around air bubbles—are parallel to the polarising directions. This reflects anticlinic or non-tilted molecular alignment in the smectic layers. The viscosity of the B₁ phase is rather high. Applying a triangular voltage (1 Hz, 150 V_{pp} μm^{−1}) perpendicularly to the sample substrates does not influence the texture, *e.g.* doesn't cause any brush movement or birefringence change.

In the dielectric measurements, a single mode with the relaxation frequency in the MHz region was found in the liquid crystalline as well as in the isotropic liquid phases. This seems to be due to the non-collective rotation of the molecules or some of their parts. The mode strength is $\Delta\epsilon \sim 3$ and becomes slightly higher in the region of the B₆ phase (Fig. 7). The molecular movement, thus the mode, is quenched in the crystalline phase.

The X-ray studies of a powdered sample of the B₁ phase reveal few low angle reflections²² (Fig. 8). These signals match a centred rectangular crystallographic lattice (Table 6). Among the registered signals, there is the (210) reflection, revealing a broken glide symmetry of the structure, which results from the non-equivalent scattering centres in the rectangular lattice—the molecule in the middle of the cell is a mirror image of the molecules in the cell corners. The dimension $b = 51$ Å of the crystallographic unit cell is related to the full molecular length, which is estimated by molecular modelling ($L = 52.8$ Å). The dimension $a = 111.6$ Å is rather large.²² In the B₁ phase the wide angle diffraction signal related to the liquid-like arrangement is obviously weaker and broader than in the B₇-like or B₂ phases, which points to a shorter correlation length of positional molecular ordering (Fig. 3).

For a most probable density of 1 g cm^{−3}, considering the dimensions of the crystallographic lattice (111.6×51 Å²) and the average packing distance between molecules along the columnar axis of about 5 Å, the number of molecules in the unit cell can be estimated to be around 18, which gives 9 molecules in each section of the column. This indicates an

Table 6 X-Ray diffraction signals for the B₁ phase of compound of series 1, $n = 12$, X = NO₂, and the corresponding crystallographic distances

| Signal indexes | (200) | (110) | (210) | (400) | (020) (120) | (220) | Calculated cell dimensions/Å |
|----------------------|-------|-------|-------|-------|----------------|-------|------------------------------|
| Registered signals/Å | 55.8 | 46.4 | 38.1 | 27.6 | 24.9 | 23.02 | $a = 111.6$ $b = 51.0$ |
| Calculated signals/Å | 55.8 | 46.4 | 37.6 | 27.6 | 25.5 | 23.02 | |
| | | | | | 24.9 | | |

average distance of about 6.2 Å between the centres of the molecules along the 'a' axis.

The compound of series 1 ($n = 12$) having a hydrogen atom at the X position in the branches reveals a monotropic liquid crystalline phase, and thus is difficult to investigate. Its microscopic texture is not similar to any of the known LC phases. The fully developed phase is soft but very viscous.

Series 2 and 3—B₂ phase

In the compounds of series 2 and 3, the B₂ phase²³ was found to be enantiotropic for series 2 and monotropic for series 3. Similar to the B₇-like phase, a broad (a few degrees) two phase region is observed in microscopic and DSC studies at the transition to the isotropic phase. The X-ray studies (Fig. 2) confirm the simple layered structure of the B₂ phase. The measured interlayer distance is shorter than the molecular length ($d/L \sim 0.84$), in agreement with the assumed tilted structure of the phase. In the microscopic studies of a freshly prepared sample (4 μm thick) mainly orange circular domains with low birefringence ($\Delta n = 0.08$) were visible. The extinction brushes are directed along the polarising directions, showing an anticlinic molecular organisation (Fig. 9a). Application of an electric field moves the extinction brushes and raises the birefringence, due to the rebuilding of the phase structure from anticlinic–antiferroelectric to synclinic–ferroelectric. The brush tilt saturates at an angle of 35.5° for a field of 4.9 V μm⁻¹ (Fig. 9b) when the domains reveal a blue–green colour that corresponds to a birefringence of $\Delta n = 0.17$. Increasing the applied field to 7 V μm⁻¹ still raises the birefringence to $\Delta n = 0.23$. This suggests a strong Kerr effect *i.e.* enhancement of the orientational order parameter S induced by the electric field. Raising the electric field to almost 12 V μm⁻¹ does not change the birefringence. Decreasing the electric field reverses the switching process.

In the fresh sample, there are also some small blue colour circular domains with extinction brushes inclined from the polarising directions, showing the presence of a synclinic molecular organisation. Their estimated birefringence is $\Delta n = 0.16$, which is similar to that of the domains with saturated brush tilt under

an electric field. In the thinner sample (2 μm), only the synclinic domains were observed. The application of a low d.c. electric field to the thin sample (of the order of 10 V μm⁻¹) orients extinction brushes along the polarising directions and lowers the birefringence without any destruction of the texture details. Thus it shows switching to an anticlinic–ferroelectric state under an applied electric field. However, switching off the field does not restore the initial synclinic–antiferroelectric state; the brushes remain in their positions and the birefringence is not changed. This suggests that either the ferroelectricity is preserved or the molecules in every second layer change their dipole moment direction, rotating around their long axis, giving the anticlinic–antiferroelectric state. The latter seems more plausible as this structure is preferred in thick samples, and thus is probably thermodynamically stable. Applying an a.c. electric field smaller than 20 V_{pp} μm⁻¹ to the thus created anticlinic–antiferroelectric state does not influence it—the texture does not change. A higher alternating electric field makes some small domains switchable, between an anticlinic–antiferroelectric state at zero field, and a synclinic–ferroelectric state under an applied field.^{20,24}

The spontaneous polarization of the compounds of series 2 was found to be 540–590 nC cm⁻², which is typical for banana materials. In the dielectric measurements, a single relaxation process was observed (Fig. 10). This mode is quenched in the

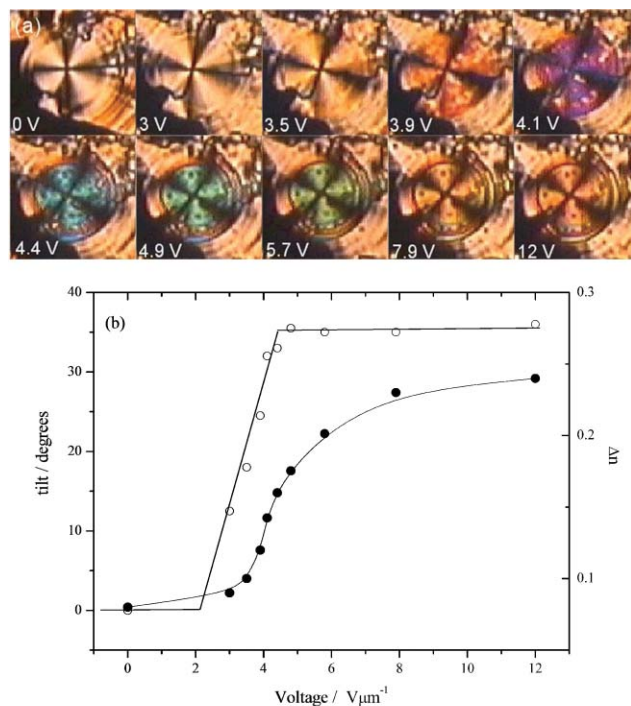


Fig. 9 (a) Circular domains in the B₂ phase under different electric fields, (b) field dependence of brush tilt and birefringence. (series 3, $n = 12$, X = Cl, sample 4 μm thick). At 0 V the structure is anticlinic–antiferroelectric.

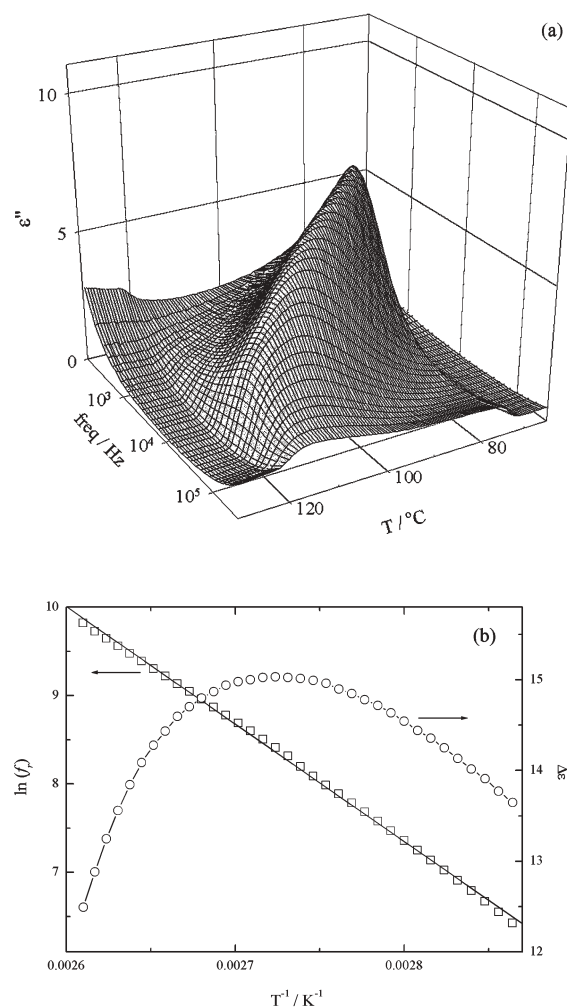


Fig. 10 (a) Temperature–frequency plot of the imaginary parts of dielectric permittivity and (b) the mode strength $\Delta\epsilon$ and the fitted mode frequency in logarithm scale as a function of inverse temperature for the B₂ phase measured on heating in planar, 2 μm thick cell (series 2, $n = 10$, X = Cl).

isotropic phase. It originates plausibly in a collective movement of molecules—the antiphase rotation of the molecules from subsequent layers.²⁴ In a sample 2 μm thick, the relaxation frequency varies with temperature, from ~ 50 kHz near the isotropisation temperature, to ~ 100 Hz close to crystallisation, within a 50 K range. The mode strength increases with decreasing temperature, and reaches $\Delta\epsilon \sim 15$. The relaxation frequency and the dielectric strength are of the same order of magnitude as for the B₂ phase in other compounds.²⁴ However the observed dependence of the relaxation frequency on temperature is much stronger than found previously,²² the corresponding activation energy being 110.3 kJ mol⁻¹.

Series 4 and 5

Lengthening the alkyl chains substituted at the central part of the molecule (at position 5, series 4) up to 5 carbon atoms changes the banana molecular shape and destroys the liquid crystalline properties. Also the banana compounds of series 5, when modified by addition of a lateral substituent at the central resorcinol ring at position 4, are not mesogenic. Only for one of the compounds (series 5 with COOC₈H₁₆ substituent in the central ring and Cl atoms in the branches) is the uniaxial nematic phase is formed.

Conclusions

A new series of bent shaped compounds containing ethylene links in the branches are presented. Similar to the frequently used imino links, they are able to transmit π electrons through the molecular branches, forming conjugated π bond systems. Moreover, due to their high symmetry, the charge density repartition between two phenyl rings should be more homogeneous than was the case for imino links.^{25,26}

The various lateral-substituents in the molecular branches induce lower melting and isotropization temperatures in comparison to the non-substituted compounds (series 1, $n = 12$, X = H). The chlorine and bromine atoms strongly promote mesomorphic phases of “banana” type. These atoms are known to be suppliers of π electrons to the aryl rings and give relatively low dipole moments. The strong van der Waals interactions accompanied by weak dipole–dipole interactions between molecules usually promote mesophases. When a nitro moiety, with a high dipole moment, is used, the LC phase is found only for the compound of series 1 with $n = 12$, X = NO₂. In the series 2 and 3, the lowering of the melting points by introduction of a *meta*-nitro group is insufficient for LC phases to be formed.

Other substituents like methoxy and dodecanoxy or at the two *meta* positions, bromine and methoxy groups, suppress the liquid crystalline properties, their bulkiness disturbing the molecular V-shape and the good lateral interactions necessary for promoting mesomorphism.

Although the stability of the liquid crystalline phase is predominately determined by lateral substituents in the banana branches, the type of phase is determined by the substituents at the central ring. The compounds studied, if they form LC phases, have a rather simple polymorphism, only one *banana* phase appears between the isotropic liquid and the solid crystal phases. With the methyl group at the 2- or 5-position, the B₂ phase is observed, while the B₇-like phase is formed when the central resorcinol ring is not substituted.

The B₂ phase is strongly sensitive to surface interactions.

The thermodynamically stable arrangement seems to be an antclinic–antiferroelectric structure, however, in a thin cell, the synclinic–ferroelectric domains are also formed. The X-ray studies of the B₂ and B₇-like phases revealed identical spectra, but nevertheless the two phases are not miscible and have quite different properties; in particular for the B₇-like phase the electrooptic response is weak and no collective mode in the dielectric studies has been found.

Acknowledgements

The studies were supported by grant BW – 1562/13/02. E. Górecka wishes to thank the CNRS and the University Louis Pasteur of Strasbourg for financial support.

References

- 1 T. Sekine, T. Niori, M. Sone, J. Watanabe, S. Choi, Y. Takanishi and H. Takezoe, *Jpn. J. Appl. Phys.*, 1997, **36**, 6455.
- 2 J. Watanabe, T. Niori, T. Sekine and H. Takezoe, *Jpn. J. Appl. Phys.*, 1998, **37**, L139.
- 3 D. Shen, S. Diele, G. Pelzl, I. Wirth and C. Tschierske, *J. Mater. Chem.*, 1999, **9**, 661.
- 4 G. Pelzl, S. Diele and W. Weissflog, *Adv. Mater.*, 1999, **11**, 707.
- 5 D. Shen, A. Pegenau, S. Diele, I. Wirth and C. Tschierske, *J. Am. Chem. Soc.*, 2000, **122**, 1593.
- 6 R. A. Reddy and B. K. Sadashiva, *Liq. Cryst.*, 2000, **27**, 1613.
- 7 V. Prasad, D. S. Rao and K. Prasad, *Liq. Cryst.*, 2001, **28**, 643.
- 8 G. Pelzl, S. Diele, A. Jákli, Ch. Lischka, I. Wirth and W. Weissflog, *Liq. Cryst.*, 1999, **26**, 135.
- 9 A. Jákli, Ch. Lischka, W. Weissflog, G. Pelzl and A. Saupe, *Liq. Cryst.*, 2000, **27**, 1405.
- 10 H. Dehne, M. Pötter, S. Sokolowski, W. Weissflog, S. Diele, G. Pelzl, I. Wirth, H. Kresse, H. Schmalfuss and S. Grande, *Liq. Cryst.*, 2001, **28**, 1269.
- 11 J. Matraszek, J. Mieczkowski, J. Szydłowska and E. Górecka, *Liq. Cryst.*, 2000, **27**, 429.
- 12 V. Prasad, *Liq. Cryst.*, 2001, **28**, 1115.
- 13 J. P. Bedel, J. C. Rouillon, J. P. Marcerou, M. Laguerre, H. T. Nguyen and M. F. Achard, *Liq. Cryst.*, 2000, **27**, 1411.
- 14 Ch.-K. Lee, J.-H. Kim, E.-J. Choi, W.-Ch. Zin and L.-Ch. Chien, *Liq. Cryst.*, 2001, **28**, 1749.
- 15 Ch.-K. Lee, A. Primak, A. Jákli, E.-J. Choi, W.-Ch. Zin and L.-Ch. Chien, *Liq. Cryst.*, 2001, **28**, 1293.
- 16 B. K. Sadashiva, H. N. Sh. Murthy and S. Dhara, *Liq. Cryst.*, 2001, **28**, 483.
- 17 W. Weissflog, H. Nadasi, U. Dunemann, G. Pelzl, S. Diele, A. Eremin and H. Kresse, *J. Mater. Chem.*, 2001, **11**, 2748.
- 18 D. S. S. Rao, G. G. Nair, S. K. Prasad, S. A. Nagamani and C. V. Yelamaggad, *Liq. Cryst.*, 2001, **28**, 1239.
- 19 N. A. Clark, D. R. Link, D. Coleman, W. G. Jang, J. Fernsler, C. Boyer, J. Zasadzinski, D. M. Walba, E. Korblova and W. Weissflog, presented at the 19th International Liquid Crystals Conference, Edinburgh, 2002.
- 20 D. M. Walba, E. Korblova, R. Shao, J. E. MacLennan, D. R. Link, M. A. Glaser and N. A. Clark, *Science*, 2000, **288**, 2181.
- 21 A. Jákli, D. Krücker, H. Sawade and G. Heppke, *Phys. Rev. Lett.*, 2001, **86**, 5715.
- 22 W. Weissflog, I. Wirth, S. Diele, G. Pelzl, H. Schmalfuss, T. Schoss and A. Würflinger, *Liq. Cryst.*, 2001, **28**, 1603.
- 23 D. R. Link, G. Natale, R. Shao, J. E. MacLennan, N. A. Clark, E. Korblova and D. M. Walba, *Science*, 1997, **278**, 1924.
- 24 G. Heppke, A. Jákli, S. Rauch and H. Sawade, *Phys. Rev. E*, 1999, **60**, 5575.
- 25 J. P. Bedel, J. C. Rouillon, J. P. Marcerou, M. Laguerre, M. F. Achard and H. T. Nguyen, *Liq. Cryst.*, 2000, **27**, 103.
- 26 J. P. Bedel, J. C. Rouillon, J. P. Marcerou, M. Laguerre, H. T. Nguyen and M. F. Achard, *Liq. Cryst.*, 2001, **28**, 128.